

Using Integrated Single-Particle ICP-MS and XANES to Reveal in Situ Speciation Transformation of Silver Nanoparticles in Cellular Environments

Yuyuan Peng,^{a,b,#} Meng Wang,^{b,c,#} Tingfeng Zhang,^{b,c} Yuchi Yao,^{b,c} Hao Fang,^{b,c} Jinke Liu,^b Xu Wang,^{b,c} Lingna Zheng,^b Xueqing Xing,^d Meng Wang,^b Xuesong Feng,^{a,*} Bing Wang,^{b,*} and Weiyue Feng^b

^aSchool of Pharmacy, China Medical University, Shenyang 110122, P. R. China

^bCAS Laboratory for Biomedical Effects of Nanomaterials and Nanosafety, Institute of High Energy Physics, Chinese Academy of Sciences, Beijing 100049, P. R. China

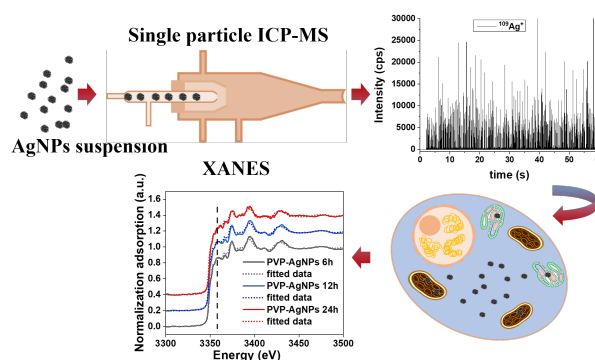
^cUniversity of Chinese Academy of Sciences, Beijing 100049, P. R. China

^dBSRF, Institute of High Energy Physics, Chinese Academy of Sciences, Beijing 100049, P. R. China

Received: January 21, 2026; Revised: February 28, 2026; Accepted: March 06, 2026; Available online: March 07, 2026.

DOI: 10.46770/AS.2026.005

ABSTRACT: Despite significant advances in analytical techniques, quantitative in situ characterization of silver nanoparticles (AgNPs) in biological systems—particularly regarding the dynamic balance between ionic and particulate silver—remains a major challenge. This study reveals that the dissolution behavior of AgNPs strongly depends on particle size and the surrounding biological medium. For example, 50 nm PVP-coated AgNPs exhibited significantly greater dissolution than 75 nm particles in both aqueous solution and DMEM medium. In aqueous environments, over 95% of silver from 50 nm NPs existed as ionic silver, compared to only about 38% from 75 nm NPs. In DMEM, a dynamic equilibrium was established, characterized by the concurrent dissolution of primary particles and the formation of new particulate species, leading to continuous fluctuations in particle number and ionic silver concentration over time. After 48 h of incubation, the released ionic silver accounted for approximately 38.4% from 50 nm particles and 26.2% from 75 nm particles. Chemical speciation analysis via synchrotron radiation-based X-ray absorption near edge structure (XANES) spectroscopy further demonstrated that intracellular silver underwent progressive transformation from the original AgNPs into Ag₂S nanoparticles, reaching a conversion ratio of 61.9% at 12 h, along with minor formation of AgCl. This transformation was closely linked to the acidic intracellular milieu and interactions with biological ligands. Although no marked cytotoxicity was observed within the first 24 h of exposure, the gradual intracellular accumulation of transformation products, particularly Ag₂S nanoparticles, eventually led to mild cytotoxic effects. These findings collectively underscore that the biological impact of AgNPs is fundamentally governed by their intracellular chemical transformation dynamics.



INTRODUCTION

The biological and environmental fate of engineered nanomaterials is fundamentally driven by their dynamic chemical transformations in complex media. Understanding these processes is therefore critical for accurately assessing their functionality,

persistence, and toxicity. Silver nanoparticles (AgNPs) are among the most extensively studied nanomaterials in nanomedicine,^{1,2} personal care products, and functional textiles, owing to their exceptional antiviral,³ antibacterial,⁴ antifungal,⁵ antitumor,⁶ and anti-inflammatory properties. However, the safe and effective deployment of AgNPs has been hindered by concerns over their colloidal instability⁷ and potential biological toxicity.⁸⁻¹⁰

Once introduced into biological systems, AgNPs undergo environment-dependent transformations, including dissolution, chlorination, and sulfidation.^{11–13} These reactions convert the original particles into diverse chemical species such as ionic silver (Ag^+), silver chloride (AgCl), and silver sulfide (Ag_2S) NPs, which each exhibit distinct bioavailability, reactivity, and toxicological profiles.¹⁴ For instance, while Ag^+ and AgCl NPs often exhibit high biological activity and toxicity, Ag_2S species are generally considered biochemically inert. Although these transformation pathways are recognized, a critical knowledge gap remains regarding how to quantitatively link the rates and extents of AgNP speciation changes within biological matrices to their subsequent cellular effects. This is primarily attributable to methodological limitations in simultaneously tracing multiple silver species in situ without perturbing the native chemical state.

In situ characterization of NPs within biological systems remains a significant challenge in analytical chemistry.¹⁵ Conventional analytical approaches for silver speciation, such as chromatographic^{16–18} or electrophoretic techniques^{19, 20} or flow field-flow fractionation^{21–23} coupled with inductively coupled plasma mass spectrometry (ICP-MS), require extensive sample preparation, including extraction and separation steps. These procedures are not only time-consuming but may also artificially alter the original speciation, compromising analytical accuracy and precluding real-time, in-situ monitoring.¹⁵ Despite emerging techniques like single-particle ICP-MS (SP-ICP-MS) and X-ray absorption near-edge spectroscopy (XANES) offer promising capabilities for the direct analysis of particles and their chemical states, robust and routine methods for quantifying AgNP transformations within living systems are still lacking.^{24, 25}

To address this challenge, we investigated the chemical speciation dynamics of polyvinylpyrrolidone (PVP)-stabilized AgNPs—a widely studied formulation of commercial relevance.²⁶ Leveraging SP-ICP-MS as a key analytical tool, we performed simultaneous, separation-free quantification of ionic and particulate silver in both simple aqueous solutions and a complex biological medium (DMEM). Furthermore, we tracked the intracellular transformation of AgNPs in real time. Our results demonstrate that AgNP fate is highly medium-dependent: rapid dissolution predominates in aqueous environments, whereas particles remain largely stable in DMEM. Notably, intracellular AgNPs were preferentially transformed into inert Ag_2S nanoparticles and subsequently expelled from cells. These findings not only clarify the environment-dependent biological pathways of AgNPs but also establish an analytical framework for the in-situ quantification of nanomaterial transformations, thereby facilitating a more accurate correlation between speciation and toxicological outcomes.

MATERIALS AND METHODS

Materials. PVP-functionalized silver nanoparticles (AgNPs; 50 nm and 75 nm) were purchased from NanoComposix. Ultrapure water (Milli-Q® water, Millipore, USA) was used throughout all experiments. High-glucose Dulbecco's Modified Eagle Medium (DMEM) was obtained from HyClone (Thermo Scientific, Waltham, MA, USA). Fetal bovine serum (FBS) and trypsin-EDTA were purchased from Gibco (Thermo Fisher Scientific, USA).

Analysis of Dissolved Ions and Particulate State of AgNPs.

Following daily instrumental optimization, analyses of blanks (water blanks), Ag^+ ionic solutions, and AgNPs were performed. A series of Ag^+ standard solutions (0, 0.01, 0.1, 0.5, 1 ppb) was used to establish a calibration curve for quantifying dissolved ionic silver. NIST 8013 gold nanoparticles (AuNPs; 2×10^5 particles/mL) were used as a reference material to determine the nebulization efficiency. Between sample runs, the introduction system was rinsed with 5% HNO_3 (60 s) followed by ultrapure water (15 s). AgNP suspensions (approximately 2×10^5 particles/mL) in ultrapure water and in DMEM supplemented with 10% FBS were analyzed after 6, 12, 24, and 48 h of incubation. For AgNPs in DMEM, all samples were centrifuged at 12,000 rpm for 20 min, and the resulting pellet was then diluted with ultrapure water prior to analysis. For SP-ICP-MS data processing, an iterative algorithm based on a five-standard-deviation (5σ) threshold was applied to distinguish single-particle events from background signals. Briefly, the mean and standard deviation (σ) of the entire dataset were calculated; signals exceeding the mean by 5σ were identified as particle events. The instrumental and data acquisition parameters for SP-ICP-MS are summarized in Table 1. For quantitative analysis of ionic Ag, the total Ag concentration was determined by digesting 0.2 mL of a diluted nanoparticle suspension ($5 \mu\text{g/mL}$). To quantify the dissolved ionic Ag fraction, 1 mL of the nanoparticle suspension ($5 \mu\text{g/mL}$) was centrifuged at 12,000 rpm for 1 h, after which 0.2 mL of the supernatant was collected for digestion. The digestion procedure was as follows: 3 mL of MOS-grade concentrated nitric acid was added to the sample in a small quartz beaker, which was then heated at 180 °C for approximately 1.5 h under reflux (with a cover). The cover was subsequently removed, and the acid was evaporated for 10–30 min

Table 1. Instrumental and data acquisition parameters for SP-ICP-MS

Instrumental parameters	Values
ICP RF power	1300 W
Plasma gas flow rate	18 L/min
Auxiliary gas flow rate	0.90 L/min
Nebulizer gas flow rate	0.88 L/min
Sample uptake rate	0.35 mL/min
Acquisition mode	Peak hopping
Sweeps	1
Dwell time	5 ms
Readings per replicate	20,000
Isotope determined	¹⁰⁷ Ag
Acquisition time	60 s

until nearly dry. The residue was stepwise diluted and recovered with 2% HNO₃, adjusted to a final weight of approximately 2 g, and quantified via ICP-MS. The dissolved ionic Ag fraction was calculated as the ratio of dissolved Ag to total Ag.

For particle size analysis, the transport efficiency was first determined using a 60 nm gold nanoparticle reference material. This value, combined with the calibration curve obtained from Ag⁺ standard solutions, was used to quantify the particle size.

Quantitative Analysis of Single-Cellular Uptake of AgNPs.

The cellular uptake experiment aimed to obtain a suitable treatment time for investigating the speciation transformation after cellular accumulation over an extended period. The mouse macrophage cell line RAW 264.7 was cultured in DMEM supplemented with 10% FBS and 1% penicillin–streptomycin at 37 °C in a 5% CO₂ atmosphere. Cells were harvested during the exponential growth phase via trypsin digestion. Subsequently, cells were exposed to 2 mL of medium containing 10 ppm PVP-AgNPs for 4, 12, 24, or 48 h to observe the progressive internalization process. After incubation, cells were collected by centrifugation at 1200 rpm for 3 min and washed three times with 0.9% NaCl solution. Finally, the cells were digested for analysis of intracellular Ag content.

Characterization of Intracellular Ag Chemical Species. To investigate the chemical forms of intracellular silver, cell samples were prepared for X-ray absorption near-edge structure (XANES) analysis. A total of 5×10^6 cells were pelleted by centrifugation, rinsed three times with PBS, and lyophilized to form a dry pellet, which was then transferred to a sealed tube. Prior to XANES measurement, the dried cell samples were pressed into flat pellets mounted on adhesive tape (3M). Silver K-edge XANES spectra were primarily recorded at beamline 1W1B of the Beijing Synchrotron Radiation Facility (BSRF), China. Transmission mode was used to collect spectra for reference compounds (Ag₂S, Ag₂O, AgCl, AgNO₃) and AgNP suspensions (10%, w/w). Fluorescence mode, using a 32-element germanium solid-state detector, was employed to acquire XANES spectra from AgNP-exposed cells. All XANES spectra were normalized to facilitate comparison across samples, measurement modes, and facilities. The preprocessed data were then subjected to linear combination fitting (LCF) using Athena (part of the IFEFFIT package, Consortium for Advanced Radiation Sources, University of Chicago) to quantify the proportions of different silver species.

Cytotoxicity Assay. Cell viability was assessed using the Cell Counting Kit-8 (CCK-8; Beyotime Biotech., Shanghai, China). Cells were seeded into 96-well plates at a density of 1.0×10^4 cells per well, with five replicate wells per group. Upon reaching 80–90% confluence, cells were treated separately with 50 nm PVP-AgNPs or 75 nm PVP-AgNPs at concentrations of 1, 5, 10, and 50 μg/mL for 6, 12, 24, and 48 h. Blank and control groups received

only material-free medium. After the respective exposure period, the medium was removed, the cells were washed twice with material-free medium, and 100 μL of fresh medium containing 10% CCK-8 reagent was added. Following incubation in the dark for 2 h, the absorbance at 450 nm was measured using a microplate reader. Relative cell viability was expressed as percentage of the untreated control.

RESULTS AND DISCUSSION

Physicochemical Characterization of Silver Nanoparticles.

TEM analysis revealed that the two types of silver nanoparticles exhibited diameters of 55.1 ± 6.2 nm and 75.4 ± 6.9 nm, respectively (Fig. 1a). SP-ICP-MS was used to record particle events—via either pulses or transient signals—with a dwell time of 5 ms, a duration longer than the typical duration of a particle event (300–1000 μs). Both sizes of PVP-AgNPs contained dissolved ionic Ag and particulate Ag in aqueous solution, as indicated by the signal pattern measured by SP-ICP-MS (Fig. 1b).

SP-ICP-MS in combination with high-throughput particle counting with time-resolved detection capability, allows for efficient and rapid characterization of NPs on a per-particle basis. This technique not only delivers quantitative data on the mass and size of individual particles, but also simultaneously determines total particle number concentration, particle size distribution, and elemental composition in both dissolved and particulate forms.²⁸ In SP-ICP-MS Time-Resolved Analysis (TRA) mode, the transient signal intensity of the target element is monitored and depends on the amount of the element reaching the detector within the dwell time.²⁹ For a dissolved ionic solution, the signal is uniformly distributed and remains relatively stable at a given

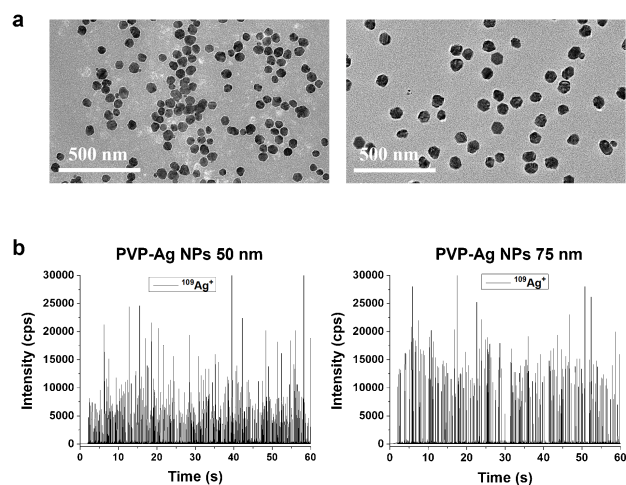


Fig. 1 Characterization of Ag nanoparticles in aqueous solution. (a) TEM image of Ag NPs. (b) Time scan of Ag NPs suspension via single particle model.

concentration. In SP-ICP-MS analysis, for a sufficiently diluted nanoparticle dispersion, the event of detecting a specific number of nanoparticles within a given measurement period or a single dwell time follows a Poisson distribution. In the study, a 5 ms dwell time was selected to completely capture a single particle signal. The probability of two-particle coincidence within a single 5 ms window was calculated to be 3.1% based on the Poisson distribution formula, indicating a relatively low likelihood of coincidence events.

$$P(k) = \frac{\lambda^k e^{-\lambda}}{k!} \quad (1)$$

Distinguishing between ionic and particulate signals in nanoparticle suspensions is crucial for accurate determination of particle number concentration and size distribution in SP-ICP-MS. To minimize false positives, a threshold of $5 \times \sigma$ was applied to differentiate particle signals from dissolved ionic signals:³⁰

$$I_D = I_B + 5 \times \sigma B \quad (2)$$

where I_D is the discrimination threshold (counts), I_B is the mean (or median) background signal (counts), and σB is the standard deviation of the background (counts). Data points below I_D were classified as dissolved ion signals, while those above were considered particle events.

Fig. 2 and Fig. 3 present the frequency distribution of signals from silver nanoparticles in aqueous medium and DMEM

respectively. In aqueous solution, 50 nm PVP-AgNPs exhibited a different single-particle signal pattern from that of 75 nm PVP-AgNPs (Fig. 2). For the 50 nm particles, signals below 900 cps were attributed to dissolved ions, while those above corresponded to single-particle events, following a near-normal distribution with a mean intensity of ~4500 cps and a total of 1180 particle events.

According to the transport efficiency (7.6%) from AuNPs (60 nm) and sample uptake velocity (0.35 mL/min), the particle events were calculated to be 2.51×10^4 /mL based on the following equation (2). This indicates that only a small amount of ionic Ag was present in the freshly prepared suspension. Over time, the number of particle events gradually decreased, dropping by 431 and 279 after 6 h and 12 h respectively, with nearly complete dissolution observed at 24 h (Fig. 2). A similar dissolution trend was noted for 75 nm PVP-AgNPs. The number of particle events decreased significantly from an initial 490 to 304 after 6 h, and further to 174 after 12 h. Statistical analysis confirmed that 50 nm PVP-AgNPs exhibited a higher dissolution percentage than PVP-Ag NPs-75 nm over 48 h, with over 95% of the Ag existing as ionic Ag (Fig. 4).

$$N_{np} = \frac{f_{np}}{Q_{sam} \times t \times \eta_n} \quad (3)$$

N_{np} : Number concentration of nanoparticle; f_{np} : number of peaks; Q_{sam} : uptake rate of nanoparticle; t : sampling time.

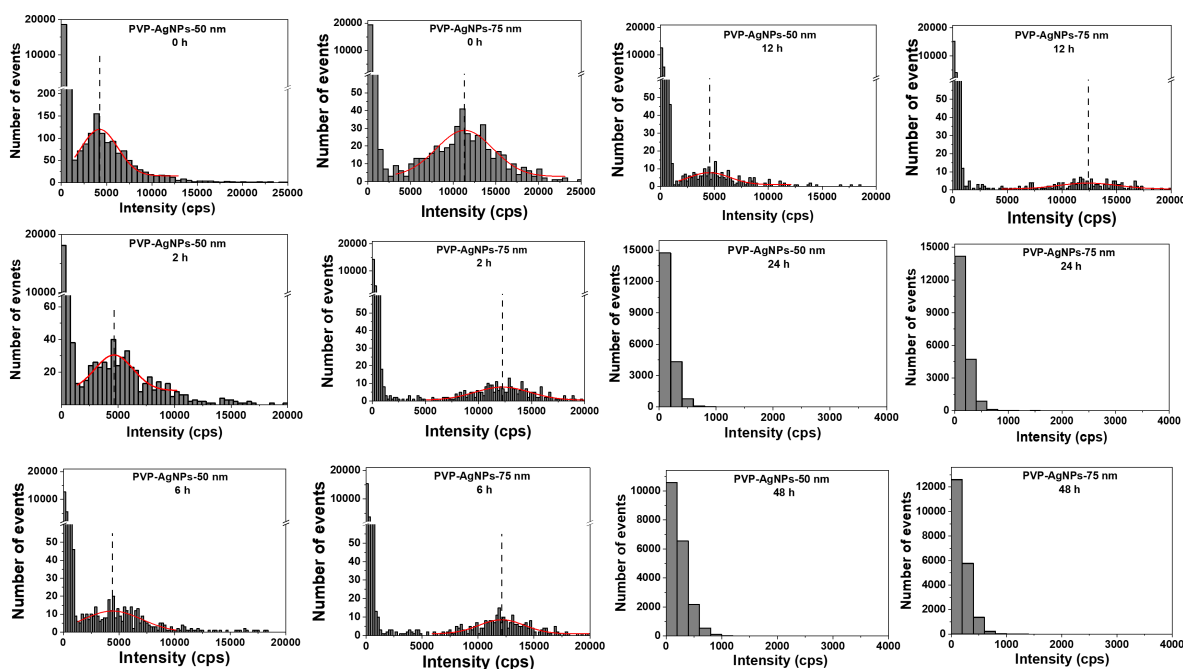


Fig. 2 Single-particle analysis of 50 nm and 75 nm PVP-AgNPs in aqueous solution.

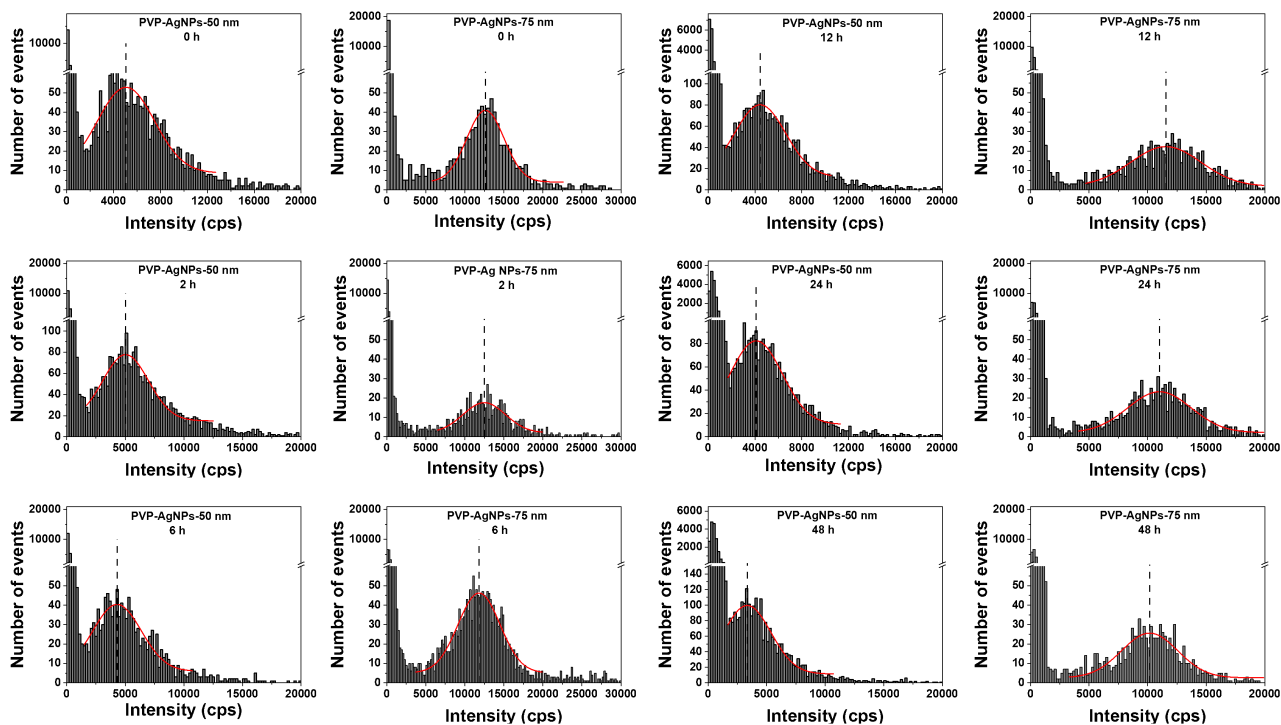


Fig. 3 Single-particle analysis of 50 nm and 75 nm PVP-AgNPs in DMEM/FBS solution.

a

PVP-AgNPs	In aqueous solution		In DMEM-F12/10%FBS	
	50 nm	75 nm	50 nm	75 nm
0 h	20.9±1.3	18.8±1.8	8.6±1.5	8.0±1.2
2 h	37.3±2.1	21.6±2.0	10.9±1.7	10.7±2.6
6 h	44.3±3.4	25.4±1.8	20.1±2.1	13.4±3.3
12 h	60.1±5.6	36.4±3.2	21.3±2.9	17.2±3.5
24 h	85.9±5.5	55.6±4.9	35.9±2.4	21.5±4.0
48 h	95±6.0	95.1±5.0	38.4±3.1	26.2±2.8

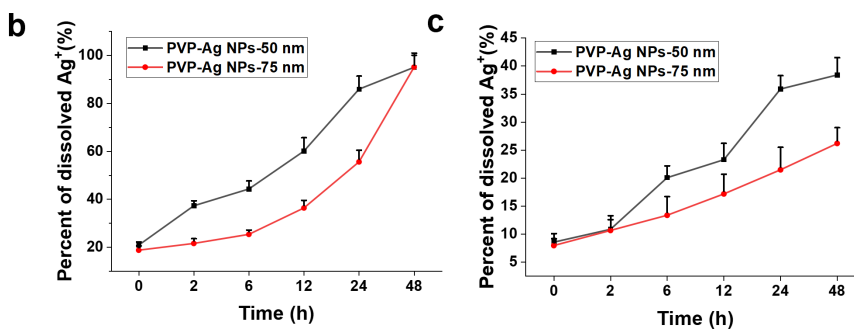


Fig. 4 Dissolution of PVP-Ag NPs in aqueous solution and DMEM/FBS. (a) Dissolution percentage of PVP-AgNPs in aqueous microenvironment and DMEM medium. (b) Dissolution kinetics curve of PVP-AgNPs in aqueous solution. (c) Dissolution kinetics curve of PVP-AgNPs in DMEM/FBS medium. $n=3$.

Figure 3 presents the frequency distribution of signals from silver nanoparticles in DMEM supplemented with FBS. The total particle events for 50 nm PVP-AgNPs decreased from an initial 1900 to 728 within the first 2 h, then increased by 2561 at 6 h and remained stable until 24 h. This pattern suggests simultaneous dissolution of primary particles and formation of new particulate species, which is consistent with previous studies.³¹ 75 nm PVP-AgNPs exhibited a similar trend: initial events decreased from 869 to 824 at 2 h, then increased to 2527 at 6 h. Further analysis indicated that the total dissolved Ag continued to rise despite the formation of new particles. After 48 h of incubation in DMEM supplemented with 10% FBS, the ionic Ag content reached approximately 38.4% and 26.2% for the 50 nm and 75 nm particles, respectively (Fig. 4).

Cellular Uptake, Speciation Transformation, and Associated Toxicity of Ag NPs. Cellular uptake of Ag NPs by RAW 264.7 cells was quantified using ICP-MS after 4, 12, 24, and 48 h of exposure. Intracellular Ag content increased progressively until 24 h, reaching a maximum of 1.60 pg/cell for 50 nm PVP-AgNPs and 1.24 pg/cell for 75 nm PVP-AgNPs (Table 2).

By 48 h, the intracellular Ag content decreased, indicating exocytosis.³¹ Chemical speciation of intracellular Ag was further investigated using SR-XANES spectroscopy (Fig. 5), focusing on 75 nm PVP-AgNPs as a representative case. Previous studies suggest that AgNPs may degrade into ions within acidic endo-

lysosomal compartments and subsequently react with biological ligands (e.g., Cl⁻, Br⁻, thiols, peptides, or proteins) to form species such as AgCl or Ag₂S.³² Silver K-edge XANES spectra were collected and fitted using linear combination analysis with reference standards: Ag NPs, Ag₂O, Ag₂S, AgCl, and AgNO₃. The spectral profiles differed notably among references; for instance, Ag₂S exhibited a broad, flat peak, while Ag NPs showed a sharp, intense peak (Fig. 5 a). The fitting results indicated that over 85% of the total silver in the DMEM/10% FBS medium was accounted for by the AgNPs (Fig. 5 a). After 6 h of incubation, intracellular Ag consisted of approximately 59.0% Ag NPs, 40.6% Ag₂S nanoparticles, and a minor amount of AgCl (Fig. 5 b & c). The proportion of Ag₂S nanoparticles peaked at 61.9% after 12 h and decreased to 41.0% by 24 h, likely due to exocytosis. Consequently, AgNPs did not exhibit significant cytotoxicity toward RAW 264.7 cells within the first 24 h of exposure (Fig. 6). However, the persistent intracellular presence of AgNPs and Ag₂S nanoparticles eventually induced mild cytotoxicity.

Table 2. Analysis of intracellular Ag content of Raw264.7 exposed to 10 ppm PVP-Ag NPs (n=3)

AgNPs	Ag/cell (pg)			
	4h	12h	24h	48h
PVP-AgNPs-50 nm	0.31±0.08	0.88±0.08	1.60±0.25	0.64±0.07
PVP-AgNPs-75 nm	0.16±0.05	0.78±0.10	1.24±0.30	0.60±0.09

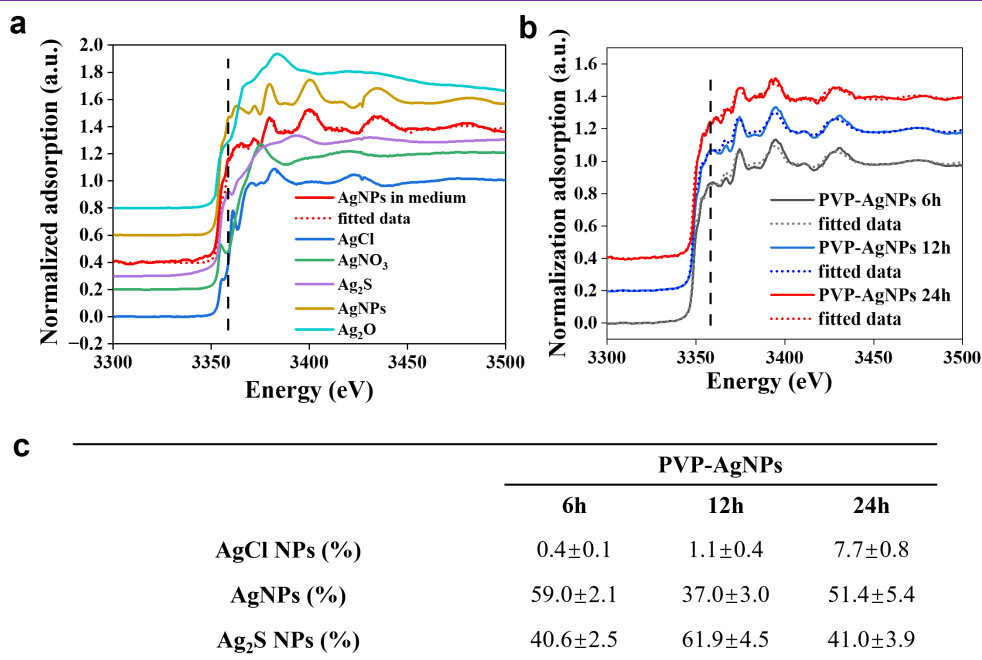


Fig. 5 Intracellular chemical speciation transformation of AgNPs. (a) Characterization of silver chemical speciation in reference samples and AgNPs as determined by silver K-edge XANES. (b) Intracellular Ag chemical speciation of the cell samples after the cellular uptake of AgNPs for 12 h and 24 h. (c) Quantitative changes in silver chemical species according to silver K-edge XANES.

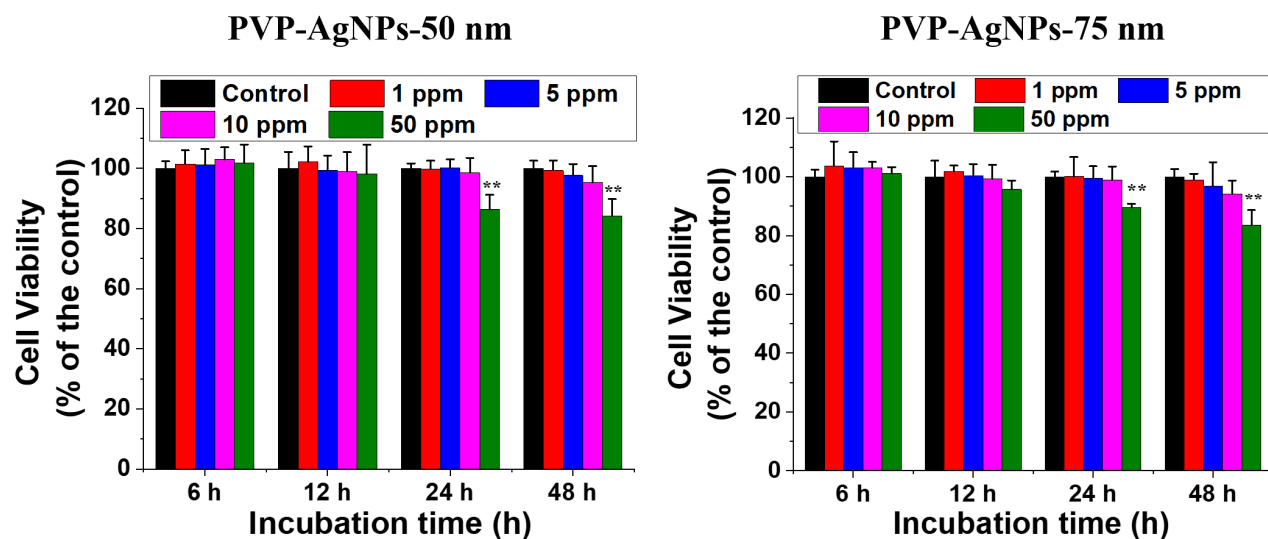


Fig. 6 Cytotoxicity assay of Raw264.7 after treatment with 10 ppm PVP-Ag NPs. $n=3$.

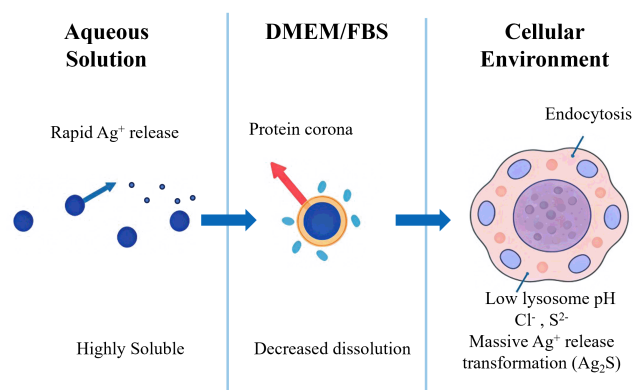


Fig. 7 Transformation of silver nanoparticles in biologically relevant media.

CONCLUSION

The dissolution behavior of Ag NPs is significantly influenced by their size and biological medium (Fig. 7). The 50 nm PVP-Ag NPs dissolved more than the 75 nm particles in aqueous and DMEM. In DMEM/FBS, a dynamic equilibrium was observed, involving simultaneous dissolution of primary particles and the formation of new particulate species, leading to concomitant changes in particle number and ionic concentration over time. After 48 h of incubation, the proportions of released ionic silver reached approximately 38.4% for the 50 nm particles and 26.2% for the 75 nm particles. The chemical speciation analysis of the 75 nm Ag NPs using synchrotron radiation XANES spectroscopy revealed that intracellular silver was progressively transformed from the original Ag NPs into Ag_2S nanoparticles (reaching a

transformation ratio of 61.9% at 12 h), accompanied by minor formation of AgCl . This transformation is closely associated with the acidic intracellular environment and reactions with biological ligands. Furthermore, Ag NPs did not exhibit significant cytotoxicity within the first 24 h of exposure. However, the persistent intracellular accumulation of transformation products, such as Ag_2S nanoparticles, eventually induced mild cytotoxicity. This indicates that the biological impact of silver nanoparticles depends on their intracellular chemical transformation.

AUTHOR INFORMATION



Bing Wang received her BSc in 1999 from Shandong University, and PhD in 2007 from the Institute of High Energy Physics, Chinese Academy of Sciences (CAS). She is an Associate Professor at the Institute of High Energy Physics, Chinese Academy of Sciences. Her research primarily focuses on applying synchrotron radiation-based analytical techniques and nuclear analysis

techniques to investigate the biological mechanisms of nanomaterials, nano-bio interfacial reactivity, and nanomedicine. She has published research findings in prestigious academic journals such as *Acc. Chem. Res.*, *ACS Nano*, *Nano Today*, *Adv. Funct. Mater.*, *Small*, *Nanotoxicology*, and *Toxicol. Lett.* She has authored or co-authored over 100 SCI-indexed papers, contributed to six monographs related to nanotoxicology. As a key member, she has participated in several national key R&D programs of the Ministry of Science and Technology related to the biological mechanisms

of nanomaterials. She has also led six projects funded by the National Natural Science Foundation of China. As a core member, she was a recipient of the '2019 CAS Outstanding Science and Technology Achievement Award' as part of the Research Group on Nanobiological Effects and Safety collective.

Corresponding Authors

* B. Wang

Email address: wangbing@ihep.ac.cn

* Xuesong Feng

Email address: voncedar@126.com

Notes

#These authors contributed equally to this work.

The authors declare no competing financial interest.

ACKNOWLEDGMENT

We thank the National Key R&D Program of China (2022YFA1207600, 2022YFA1603802), the National Natural Science Foundation of China (12275300, 12275302, and 12535020), the Beijing Natural Science Foundation (Z230008), and the directional institutionalized scientific research platform relies on Beijing Synchrotron Radiation Facility of Chinese Academy of Sciences for the grants to this research. The authors would like to acknowledge BSRF and the staff in the beamline 1W1B and 1W2A at BSRF for their assistance.

REFERENCES

1. S. Bhakya, S. Muthukrishnan, M. Sukumaran, and M. Muthukumar, *Appl. Nanosci.*, 2015, **6**, 755-766. <https://doi.org/10.1007/s13204-015-0473-z>
2. F. Ameen, S. A. AlYahya, M. A. Bakhrebah, M. S. Nassar, and A. Aljuraifani, *Res. Chem. Intermed.*, 2018, **44**, 5063-5073. <https://doi.org/10.1007/s11164-018-3409-x>
3. K. Naumenko, S. Zahorodnia, C. V. Pop, and N. Rizun, *J. Virus Erad.*, 2023, **9**, 100330. <https://doi.org/10.1016/j.jve.2023.100330>
4. S. Tang and J. Zheng, *Adv. Healthcare Mater.*, 2018, **7**, 1701503. <https://doi.org/10.1002/adhm.201701503>
5. Z. K. Xia, Q. H. Ma, S. Y. Li, D. Q. Zhang, L. Cong, Y. L. Tian, and R. Y. Yang, *J. Microbiol. Immunol. Infect.*, 2016, **49**, 182-188. <https://doi.org/10.1016/j.jmii.2014.04.013>
6. S. Mussa Farkhani, A. Asoudeh Fard, P. Zakeri-Milani, J. Shahbazi Mojarad, and H. Valizadeh, *Artif. Cells, Nanomed., Biotechnol.*, 2017, **45**, 1029-1035. <https://doi.org/10.1080/21691401.2016.1200059>
7. R. Vazquez-Munoz, N. Bogdanchikova, and A. Huerta-Saquerro, *ACS Omega*, 2020, **5**, 28441-28451. <https://doi.org/10.1021/acsomega.0c02007>
8. T. Jaswal and J. Gupta, *Mater. Today: Proc.*, 2023, **81**, 859-863. <https://doi.org/10.1016/j.matpr.2021.04.266>
9. P. Cvjetko, A. Milosic, A. M. Domijan, I. Vinkovic Vrcek, S. Tolic, P. Peharec Stefanic, I. Letofsky-Papst, M. Tkalec, and B. Balen, *Ecotoxicol. Environ. Saf.*, 2017, **137**, 18-28. <https://doi.org/10.1016/j.ecoenv.2016.11.009>
10. P. Nie, Y. Zhao, and H. Xu, *Ecotoxicol. Environ. Saf.*, 2023, **253**, 114636. <https://doi.org/10.1016/j.ecoenv.2023.114636>
11. Q. Bai, Q. Li, R. Zheng, S. Yu, Z. Hao, J. Liu, and Y. Cai, *Environ. Pollut.*, 2025, **368**, 125726. <https://doi.org/10.1016/j.envpol.2025.125726>
12. A. Malysheva, A. Ivask, C. L. Doolette, N. H. Voelcker, and E. Lombi, *Nat. Nanotechnol.*, 2021, **16**, 926-932. <https://doi.org/10.1038/s41565-021-00914-3>
13. M. Baccaro, A. K. Undas, J. de Vriendt, J. H. J. van den Berg, R. J. B. Peters, and N. W. van den Brink, *Environ. Sci.: Nano*, 2018, **5**, 1107-1116. <https://doi.org/10.1039/c7en01212h>
14. B. Purushothaman and J. M. Song, *Biomater. Sci.*, 2021, **9**, 51-69. <https://doi.org/10.1039/d0bm01576h>
15. R. B. Patil and A. D. Chougale, *Mater. Today: Proc.*, 2021, **47**, 5520-5532. <https://doi.org/10.1016/j.matpr.2021.03.384>
16. R. A. Gonzalez-Fuenzalida, Y. Moliner-Martinez, C. Molins-Legua, V. Parada-Artigues, J. Verdu-Andres, and P. Campins-Falco, *Anal. Chem.*, 2016, **88**, 1485-1493. <https://doi.org/10.1021/acs.analchem.5b04751>
17. C. A. Sotebier, S. M. Weidner, N. Jakubowski, U. Panne, and J. Bettmer, *J. Chromatogr. A*, 2016, **1468**, 102-108. <https://doi.org/10.1016/j.chroma.2016.09.028>
18. T. Karan, Z. Gonulalan, R. Erenler, U. Kolemen, and O. Eminagaoglu, *J. Mol. Struct.*, 2024, **1296**, 136836. <https://doi.org/10.1016/j.molstruc.2023.136836>
19. A. T. Sutton, R. D. Arrua, S. C. Thickett, E. Lombi, and E. F. Hilder, *Environ. Sci.: Nano*, 2019, **6**, 1351-1362. <https://doi.org/10.1039/c9en00014c>
20. H. Qu, T. K. Mudalige, and S. W. Linder, *J. Chromatogr. A*, 2016, **1429**, 348-353. <https://doi.org/10.1016/j.chroma.2015.12.033>
21. M. Wang, L. Zheng, B. Wang, P. Yang, H. Fang, S. Liang, W. Chen, and W. Feng, *Chin. Chem. Lett.*, 2022, **33**, 3484-3487. <https://doi.org/10.1016/j.ccllet.2022.03.098>
22. R. Jian, K. Hu, Q. Guo, L. Zhao, H. Yu, and K. Huang, *Microchem. J.*, 2022, **175**, 107164. <https://doi.org/10.1016/j.microc.2021.107164>
23. P. Chang, L. Zheng, B. Wang, M. Chen, M. Wang, J. Wang, and W. Feng, *Atom. Spectrosc.*, 2022, **43**, 255-265. <https://doi.org/10.46770/as.2022.108>
24. H. Cui, H. Cui, T. Wang, J. Hong, L. Lei, and S. Wei, *Atom. Spectrosc.*, 2023, **44**, 343-353. <https://doi.org/10.46770/as.2023.202>
25. H. Zhao, J. Zhao, J. Zhang, C. Hu, Y. Liu, W. Zhao, and Z. Hu, *Atom. Spectrosc.*, 2024, **45**, 67-73. <https://doi.org/10.46770/as.2024.001>
26. N. Bogdanchikova, J. N. Díaz de León, M. H. Fariás Sánchez, G. A. Hirata Flores, M. Á. Pastrana Corral, A. Pestryakov, and D. Garibo Ruiz, *Nano-Struct. Nano-Objects*, 2026, **45**, 101601. <https://doi.org/10.1016/j.nanoso.2025.101601>
27. Z. Chen, J. W. Chang, C. Balasanthiran, S. T. Milner, and R. M. Rioux, *J. Am. Chem. Soc.*, 2019, **141**, 4328-4337. <https://doi.org/10.1021/jacs.8b11295>

28. X. Lin, N. Yan, Y. Yang, Z. Wu, Y. Xu, and X. Yu, *Chin. J. Inorg. Anal. Chem.*, 2024, **14**, 896-910.
<https://doi.org/10.3969/j.issn.2095-1035.2024.07.006>
 29. A. L. M. de Souza, T. Pedron, R. M. Pereira, F. F. da Silva, C. N. Lange, A. B. Seabra, and B. L. Batista, *J. Trace Elem. Miner.*, 2023, **4**, 100054. <https://doi.org/10.1016/j.jtemin.2023.100054>
 30. F. Laborda, A. C. Gimenez-Ingalaturre, E. Bolea, and J. R. Castillo, *Spectrochim. Acta*, 2020, **169**, 105883.
<https://doi.org/10.1016/j.sab.2020.105883>
 31. L. Wang, T. Zhang, P. Li, W. Huang, J. Tang, P. Wang, J. Liu, Q. Yuan, R. Bai, B. Li, K. Zhang, Y. Zhao, and C. Chen, *ACS Nano*, 2015, **9**, 6532-6547. <https://doi.org/10.1021/acs.nano.5b02483>
 32. Y. Yin, W. Xu, Z. Tan, Y. Li, W. Wang, X. Guo, S. Yu, J. Liu, and G. Jiang, *Environ. Pollut.*, 2017, **220**, 955-962.
<https://doi.org/10.1016/j.envpol.2016.10.081>
-